An approximate analysis of dry-friction-induced stick-slip vibratons by a smoothing procedure

Nonlinear Dynamics **19:** 157–169, 1999.

An Approximate Analysis of Dry-Friction-Induced Stick-Slip Vibrations by a Smoothing Procedure *

B. L. VAN DE VRANDE, D. H. VAN CAMPEN, and A. DE KRAKER
Department of Mechanical Engineering, Eindhoven University of Technology, P.O. Box 513, 5600 MB Eindhoven, The Netherlands

(Received: 5 November 1997; accepted: 9 December 1998)

Abstract. This paper deals with a systematic procedure to find both stable and unstable periodic stick-slip vibrations of autonomous dynamic systems with dry friction. In this procedure, the discontinuous friction forces are approximated by smooth functions. Using the simple shooting method with a stiff-ODE solver, in combination with a path following algorithm, branches of periodic solutions are computed for a changing design variable. For testing purposes, both 1 and 2-DOF autonomous block-on-belt models and a 1-DOF autonomous drill string model from literature are investigated. Comparison of the results shows that the smoothing procedure accurately describes the behavior of the discontinuous systems. The proposed procedure can also easily be applied to more complex MDOF models, as well as to nonautonomous dynamic systems.

Keywords: Stick-slip vibrations, dry friction, discontinuous systems, smoothing.

Nomenclature

c_1	=	torsional damping [Nms]
e	=	relative error
F, F_i	=	friction forces [N]
F_N	=	normal force [N]
F_s, $F_{\mathrm{s},i}$	=	maximum static friction forces [N]
F^*, F_i^*	=	nondimensional friction forces
h, h_i	=	nondimensional step lengths
J_1	=	mass moment of inertia [kgm^2]
k, k_i, k_c	=	translational and torsional stiffnesses [N/m] and [Nm]
m, m_i	=	masses [kg]
P	=	nondimensional period
t	=	time [s]
T	=	friction torque [Nm]
T_s	=	maximum static friction torque [Nm]
T^*	=	nondimensional friction torque
v_dr	=	driving belt velocity [m/s]
v_rel	=	relative velocity [m/s]
V_dr	=	nondimensional driving belt velocity
V_rel, $V_{\mathrm{rel},i}$	=	nondimensional relative velocities
x, x_i	=	displacements [m]
X, X_i	=	nondimensional displacements
α	=	stiffness ratio
β	=	maximum static friction force ratio
γ	=	nondimensional parameter in dynamic friction coefficient

* Contributed by Professor A. K. Bajaj.

δ = parameter in dynamic friction coefficient [s/m]
ε = accuracy parameter
ζ = damping coefficient
η = nondimensional angular velocity
θ = nondimensional friction torque difference
κ = accuracy parameter
μ = dynamic friction coefficient
μ_0 = constant static friction coefficient
τ = nondimensional time
φ = relative angular displacement
φ_i = angular displacements
φ_{eq} = equilibrium relative angular displacement
ψ = relative angular displacement
ω = angular eigenfrequency [1/s]
Ω_2 = constant angular velocity [1/s]

1. Introduction

In engineering practice, dry friction often causes undesirable side effects. It can induce self-sustained stick-slip vibrations that produce noise and shorten the lifespan of mechanical parts. Examples of such vibrations are observed in grating brakes and chattering machine tools. Some stick-slip vibrations experienced in everyday life are squeaking pieces of chalk and creaking doors. Ibrahim [6] gives a comprehensive account of the main theorems and mechanisms developed in literature concerning friction-induced noise and vibration.

The general model to describe a dry friction force is given by

$$\begin{cases} |F| \le \mu_0 F_{\text{N}} = F_{\text{s}} & \text{if } v_{\text{rel}} = 0 \text{ (stick)}, \\ F = -\mu F_{\text{N}} \operatorname{sgn} v_{\text{rel}} = -(\mu/\mu_0) F_{\text{s}} \operatorname{sgn} v_{\text{rel}} & \text{if } v_{\text{rel}} \neq 0 \text{ (slip)}, \end{cases} \tag{1}$$

where F is the friction force, μ_0 the constant static friction coefficient, F_{N} the normal force, F_{s} the maximum static friction force, v_{rel} the relative velocity, and μ the dynamic friction coefficient, which is a function of $|v_{\text{rel}}|$. In literature, several models are proposed that describe this dependence of the dynamic friction coefficient on the relative velocity. Coulomb's classic friction law assumes μ to be constant and less than or equal to μ_0. In most other models, μ is a decreasing function of $|v_{\text{rel}}|$, which has also been observed in experiments [10].

The motivation for this work is the torsional stick-slip vibration that occurs in oil exploration drill strings [7, 11]. A drill string mainly consists of a slender steel tube called the drill pipe (see Figure 1). At the lower part of the drill string, drill collars (thick walled pipes) and stabilizers (cylindrical elements that fit loosely in the bore hole) are used to avoid buckling. At the top, the drill string is supported by a drilling rig and rotated by the rotary table. Between the drill bit, the drill collars, and the stabilizers on the one hand, and the soil on the other hand, dry friction occurs, causing the observed stick-slip vibration. During this vibration, the angular velocity of the rotary table is approximately constant, whereas the velocity at the bit varies between zero (the stick phase) and a velocity that is several times higher than the average velocity at the top (during the slip phase). Because the torsional stick-slip vibration can result in failure of drilling components, control systems are needed to suppress it. Therefore, a numerical model that accurately describes the behavior of the drill string is essential.

Applying the model of Equation (1) yields a set of discontinuous ODEs for a dynamic system with dry friction. A procedure is proposed to systematically find stable and unstable

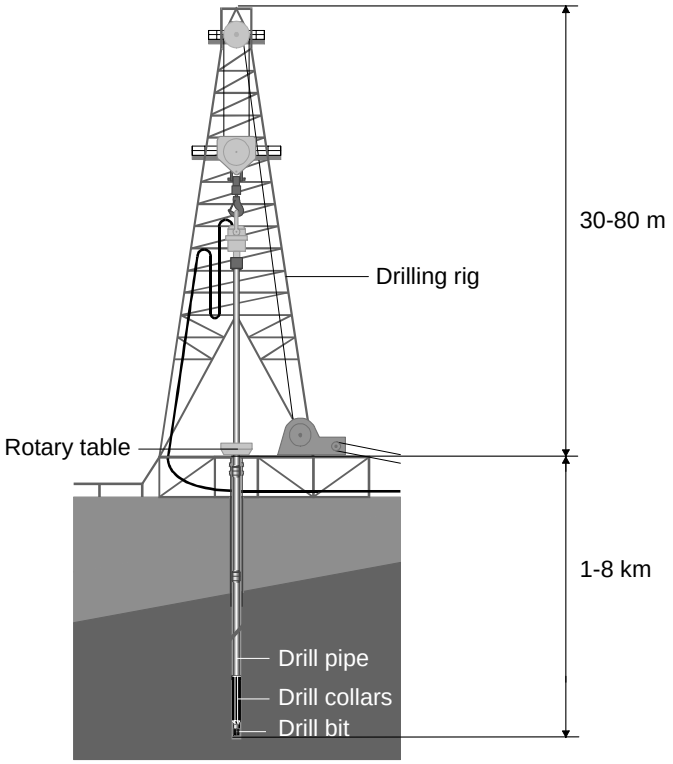

Figure 1. Drilling rig.

periodic stick-slip vibrations of autonomous dynamic systems with dry friction, using the module STRDYN of the finite element code DIANA [1]. This module contains several numerical algorithms to investigate finite element models with local nonlinearities such as dry friction. As for most bifurcation codes, these nonlinearities have to be sufficiently smooth, so the friction forces are approximated by smooth functions. The simple shooting method [9, 12] with a stiff-ODE solver is used in combination with a path following algorithm [2] to compute branches of periodic solutions for a changing design variable of the system.

To test the smoothing procedure, it is applied to both 1 and 2-DOF autonomous block-on-belt models and a 1-DOF autonomous drill string model from literature. It is concluded that, using this procedure, systems with dry friction can successfully be modeled in a bifurcation code such as STRDYN and that the procedure can also easily be applied to more complex MDOF models, as well as to nonautonomous dynamic systems.

2. Block-on-Belt Models

2.1. 1-DOF MODEL

The 1-DOF block-on-belt model from Galvanetto et al. [3] is depicted in Figure 2a. The mass m is attached to inertial space by the spring k, and is riding on a driving belt that is moving at the constant velocity v_{dr}. The displacement of m is denoted by x. Between the mass and the belt, dry friction occurs with friction force F.

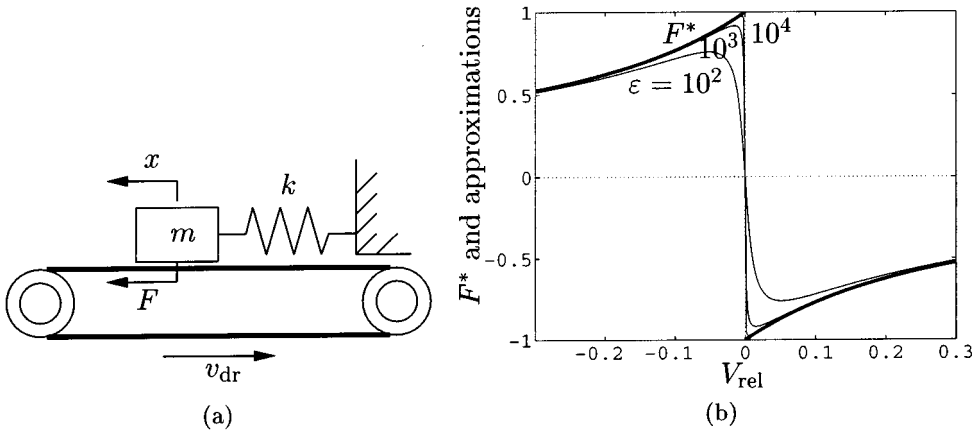

Figure 2. (a) 1-DOF block-on-belt model and (b) F^* and approximations.

The nondimensional equation of motion is given by

$$X'' + X = F^*, \tag{2}$$

where a prime denotes a differentiation with respect to $\tau = \omega t$, $\omega = \sqrt{k/m}$, t is time, $X = kx/F_s$, F_s is the maximum static friction force, and $F^* = F/F_s$. The dynamic friction coefficient is given by $\mu = \mu_0/(1 + \delta|v_{rel}|) = \mu_0/(1 + \gamma|V_{rel}|)$, where the positive parameter δ measures the rate at which μ decreases with an increase in $|v_{rel}|$, $v_{rel} = \dot{x} - v_{dr}$, an overdot denotes a differentiation with respect to t, $\gamma = F_s\delta/\sqrt{km}$, $V_{rel} = X' - V_{dr}$, and $V_{dr} = \sqrt{km}\, v_{dr}/F_s$. Though μ approaches zero as $|V_{rel}|$ increases, which clearly is not a good physical model, it will not become less than about $0.25\mu_0$ because V_{dr} will be chosen less than or equal to 0.2, causing a maximum $|V_{rel}|$ of about 1.

F^* is given by

$$\begin{cases} |F^*| \le 1 & \text{if } V_{rel} = 0, \\ F^* = -\operatorname{sgn} V_{rel}/(1 + \gamma|V_{rel}|) & \text{if } V_{rel} \neq 0, \end{cases} \tag{3}$$

and approximated by the smooth function

$$-(2/\pi)\arctan(\varepsilon V_{rel})/(1 + \gamma|V_{rel}|), \tag{4}$$

where ε is the accuracy parameter. Following Galvanetto et al. [3], γ is chosen equal to 3. Figure 2b shows F^* (thick line) and the smooth approximations with $\varepsilon = 10^2$, 10^3, and 10^4. Increasing ε improves the approximation but causes a steep slope at $V_{rel} = 0$ given by $-2\varepsilon/\pi$. This makes Equation (2) stiff, so the backward differentiation formulas (BDFs, [5]) are used for numerical integration in the shooting method.

In Figure 3a, the stable periodic solutions at $V_{dr} = 0.2$ are shown for the approximations with $\varepsilon = 10^2$, 10^3, and 10^4. An 'exact' solution to the discontinuous model is found by the brute-force approach, i.e., numerical integration until a (stable) steady state is reached, using Hénon's method [4] to locate the stick-to-slip and slip-to-stick transitions (see appendix A). Hénon's method cannot be used in combination with the shooting method and the path following algorithm in a bifurcation code such as STRDYN, and also becomes very laborious for MDOF systems. The 'exact' solution is shown in Figure 3a by the thick line and is used to investigate the accuracy of the approximations.

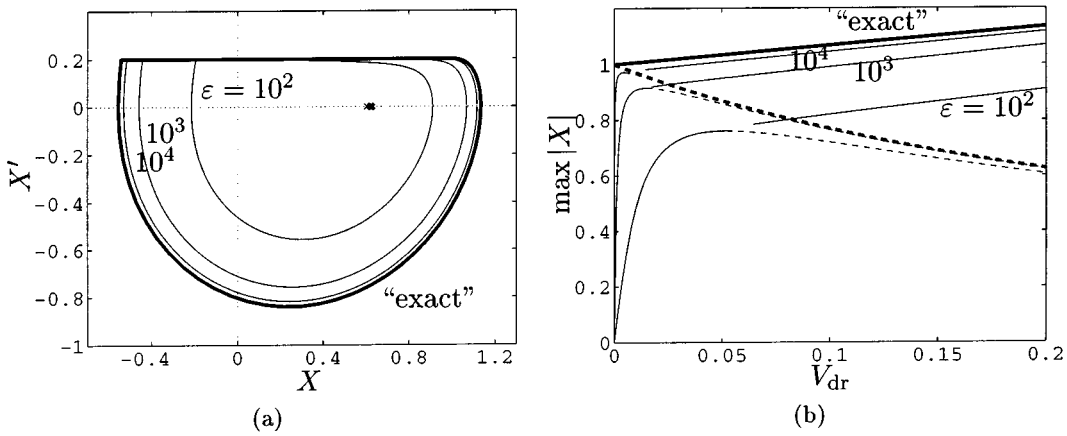

Figure 3. (a) Periodic solution at $V_{\rm dr} = 0.2$ and (b) max $|X|$ as a function of $V_{\rm dr}$.

Table 1. Error e of the approximate solutions at $V_{\rm dr} = 0.2$.

ε	10^2	10^3	10^4	10^5	10^6
e	$2.9 \cdot 10^{-1}$	$8.9 \cdot 10^{-2}$	$2.4 \cdot 10^{-2}$	$6.2 \cdot 10^{-3}$	$1.5 \cdot 10^{-3}$

The relative error e of the approximate solutions is defined by

$$e = \sqrt{\frac{\sum_i (X_i - X_{\text{exact},i})^2 + \sum_i (X'_i - X'_{\text{exact},i})^2 + (P - P_{\text{exact}})^2}{\sum_i X^2_{\text{exact},i} + \sum_i X'^2_{\text{exact},i} + P^2_{\text{exact}}}}, \tag{5}$$

where the subscript i denotes $\tau = i\,P/N$ and $\tau = i\,P_{\text{exact}}/N$ for the approximate and 'exact' solutions, respectively, P and P_{exact} are the periods of the approximate and 'exact' solutions, respectively, the summations over i are from 0 to $N-1$, and N is the number of time points. The error is given in Table 1 as a function of ε, where N is chosen equal to 200.

Path following is performed with $V_{\rm dr}$ as the design variable, starting from the calculated approximate solutions at $V_{\rm dr} = 0.2$. Figure 3b shows max $|X|$ as a function of $V_{\rm dr}$ for the approximations with $\varepsilon = 10^2$, 10^3, and 10^4, and for the 'exact' solution found by brute force (thick line).

The equilibrium points of the approximate and discontinuous models, given by

$$X = (2/\pi)\arctan(\varepsilon V_{\rm dr})/(1 + \gamma V_{\rm dr}) \quad \text{and} \quad X = 1/(1 + \gamma V_{\rm dr}), \tag{6}$$

respectively, are also shown in Figure 3b, where solid and dashed lines represent stable and unstable branches, respectively. In Figure 3a, the positions of the equilibrium points at $V_{\rm dr} = 0.2$ are given by the x-marks. The equilibrium point of the discontinuous model (thick dashed line in Figure 3b) is unstable for all values of $V_{\rm dr}$. For the approximate models, however, at a certain value of $V_{\rm dr}$ (given in Table 2) the stability of the equilibrium point changes by a super-critical Hopf bifurcation, and the stable periodic solution is born. The approximate periodic solution branches do not reach this Hopf bifurcation because the step size in the path following algorithm becomes smaller than the user defined minimum.

Table 2. Super-critical Hopf bifurcation points.

ε	10^2	10^3	10^4	10^5	10^6
V_{dr}	$5.19 \cdot 10^{-2}$	$1.52 \cdot 10^{-2}$	$4.67 \cdot 10^{-3}$	$1.46 \cdot 10^{-3}$	$4.61 \cdot 10^{-4}$

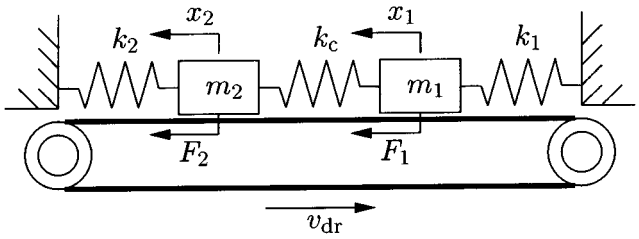

Figure 4. 2-DOF block-on-belt model.

2.2. 2-DOF MODEL

The 2-DOF block-on-belt model from Galvanetto et al. [3] is depicted in Figure 4. The masses m_1 and m_2 are riding on a driving belt that is moving at the constant velocity v_{dr}. They are connected by the spring k_c, and attached to inertial space by the springs k_1 and k_2, respectively. The displacements of m_1 and m_2 are denoted by x_1 and x_2, respectively. Between the masses and the belt, dry friction occurs with friction forces F_1 and F_2 acting on m_1 and m_2, respectively. It is assumed that $m_1 = m_2 = m$ and $k_1 = k_2 = k$.

The nondimensional equations of motion are given by

$$\begin{cases} X_1'' + X_1 + \alpha(X_1 - X_2) = F_1^*, \\ X_2'' + X_2 + \alpha(X_2 - X_1) = F_2^*, \end{cases} \tag{7}$$

where a prime denotes a differentiation with respect to $\tau = \omega t$, $\omega = \sqrt{k/m}$, t is time, $X_i = kx_i/F_{\mathrm{s},1}$, $F_{\mathrm{s},i}$ is the maximum static friction force on mass m_i, $\alpha = k_c/k$, and F_i^*=$F_i/F_{\mathrm{s},1}$.

F_1^* and F_2^* are given by

$$\begin{cases} |F_1^*| \le 1 & \text{if } V_{\mathrm{rel},1} = 0, \\ F_1^* = -\operatorname{sgn} V_{\mathrm{rel},1}/(1 + \gamma|V_{\mathrm{rel},1}|) & \text{if } V_{\mathrm{rel},1} \neq 0, \end{cases} \tag{8}$$

and

$$\begin{cases} |F_2^*| \le \beta & \text{if } V_{\mathrm{rel},2} = 0, \\ F_2^* = -\beta \operatorname{sgn} V_{\mathrm{rel},2}/(1 + \gamma|V_{\mathrm{rel},2}|) & \text{if } V_{\mathrm{rel},2} \neq 0, \end{cases} \tag{9}$$

respectively, where $V_{\mathrm{rel},i} = X_i' - V_{\mathrm{dr}}$, $V_{\mathrm{dr}} = \sqrt{km}\, v_{\mathrm{dr}}/F_{\mathrm{s},1}$ and $\beta = F_{\mathrm{s},2}/F_{\mathrm{s},1}$. F_1^* and F_2^* are approximated by the smooth functions

$$-(2/\pi)\arctan(\varepsilon V_{\mathrm{rel},1})/(1 + \gamma|V_{\mathrm{rel},1}|) \tag{10}$$

and

$$-\beta(2/\pi)\arctan(\varepsilon V_{\mathrm{rel},2})/(1 + \gamma|V_{\mathrm{rel},2}|), \tag{11}$$

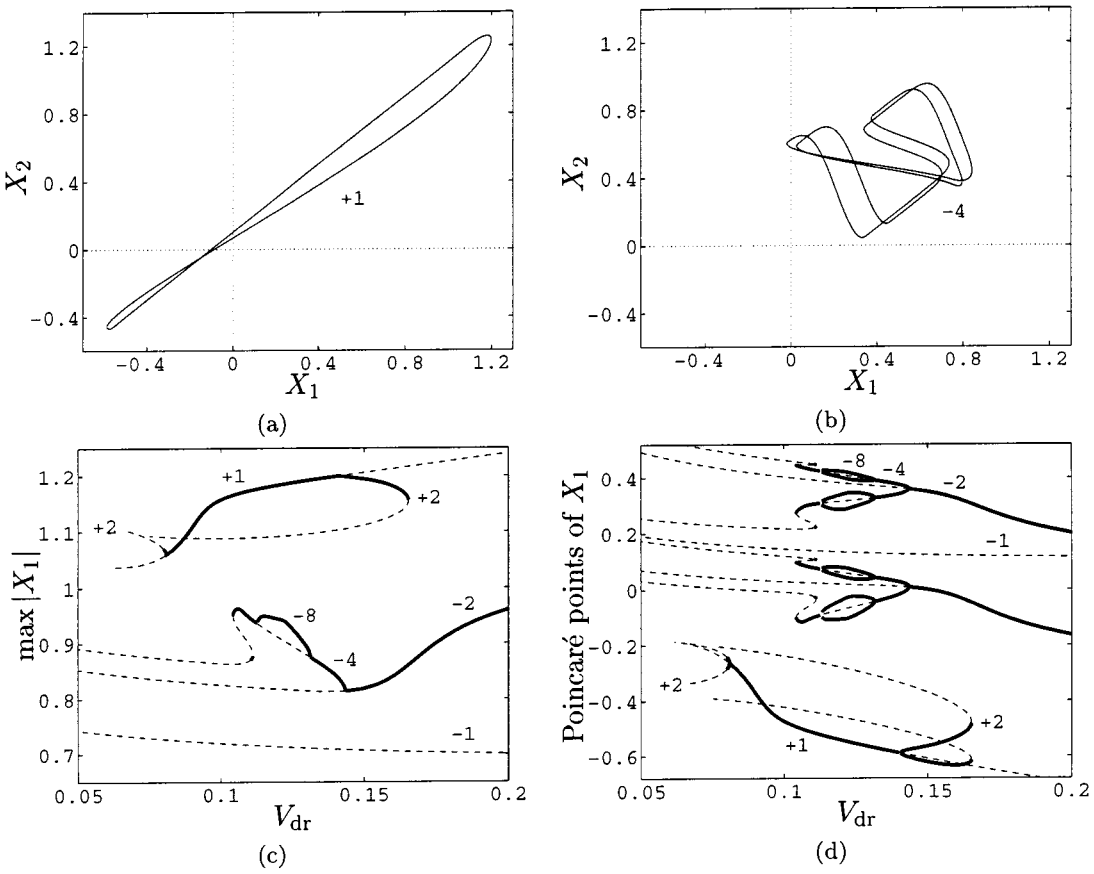

Figure 5. Stable (a) 'in phase' period-1 and (b) 'out of phase' period-4 solutions at $V_{dr} = 0.14$, and (c) max $|X_1|$ and (d) Poincaré points of X_1 as functions of V_{dr}.

respectively. As used by Galvanetto et al. [3], the following values are chosen:

$$\alpha = 1.2, \quad \beta = 1.3, \quad \gamma = 3. \tag{12}$$

According to Table 1, an acceptable accuracy is obtained with $\varepsilon = 10^5$, so this value is used for the 2-DOF model.

Figures 5a and 5b show two stable solutions at $V_{dr} = 0.14$, where X_2 is plotted against X_1. Figure 5a represents an 'in phase' period-1 solution, where 'in phase' means that the masses are roughly moving in the same direction. A period-n solution is defined as a periodic solution that crosses the Poincaré section, defined by $X_1' = 0$, n times from a negative to a positive value during its minimum period. Figure 5b shows an 'out of phase' period-4 solution where the two masses are roughly moving in opposite directions.

Path following is performed with V_{dr} as the design variable. Figures 5c and 5d show max $|X_1|$ and the Poincaré points of X_1, respectively, where thick solid lines and dashed lines represent stable and unstable solutions, respectively. Also, $+n$ and $-n$ identify 'in phase' and 'out of phase' period-n solution branches, respectively. Both for low driving belt velocities and higher period solution branches, the step size becomes very small, causing long CPU times.

Table 3. Bifurcations in 2-DOF block-on-belt model.

Branch	Bifurcation	V_{dr}
$+1$	super-critical flips	0.081 and 0.141
$+2$ (left)	flip	0.080
$+2$ (right)	cyclic fold	0.165
-2	super-critical flip	0.144
-4	super-critical flips	0.113 and 0.132
	flip	0.1106
	cyclic folds	0.104 and 0.1112

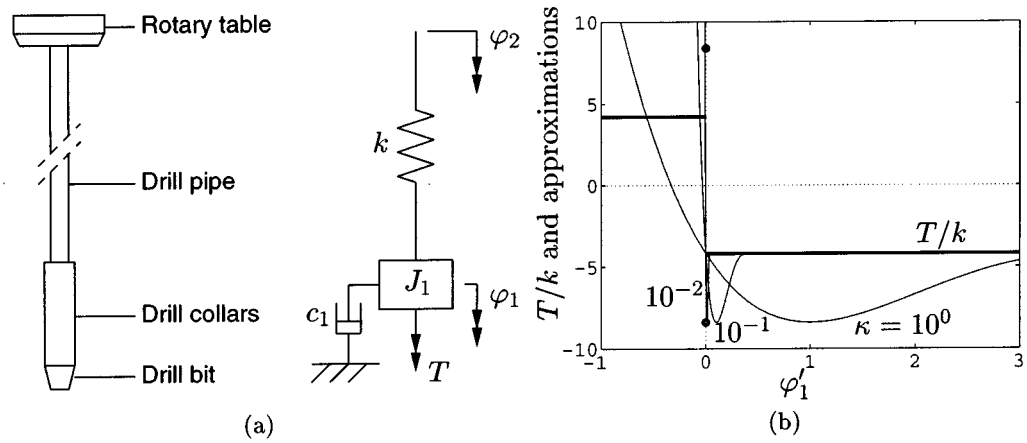

Figure 6. (a) Drill string model and (b) T/k and approximations.

The bifurcation diagram of Figure 5d corresponds to the diagram from Galvanetto et al. [3], but in addition unstable branches and an extra stable -4 branch between $V_{\mathrm{dr}} = 0.1106$ and 0.1112 are found. The observed bifurcations are listed in Table 3.

3. Drill String Model

The 1-DOF drill string model for investigating torsional stick-slip vibrations from Jansen [7] is depicted in Figure 6a. The drill pipe is modeled by the linear torsional spring k. The drill collars are assumed to be rigid and modeled as the equivalent mass moment of inertia J_1, also taking into account the mass moment of inertia of the drill pipe. Viscous damping is introduced by the linear torsional damper c_1. The angular displacement of the bit and the drill collars is represented by φ_1; the angular displacement of the rotary table by φ_2. Between J_1 and inertial space dry friction occurs with friction torque T, given by

$$\begin{cases} |T| \le T_{\mathrm{s}} & \text{if } \dot{\varphi}_1 = 0, \\ T = -(\mu/\mu_0) T_{\mathrm{s}} \operatorname{sgn} \dot{\varphi}_1 & \text{if } \dot{\varphi}_1 \neq 0, \end{cases} \tag{13}$$

where T_{s} is the maximum static friction torque and an overdot denotes a differentiation with respect to time t. Coulomb friction is assumed with $\mu = \mu_0/2$.

Choosing $\varphi = \varphi_2 - \varphi_1$ as the generalized coordinate and assuming that the rotary table is rotating at the constant velocity $\Omega_2 > 0$, the equation of motion is given by

$$J_1\ddot{\varphi} + c_1\dot{\varphi} + k\varphi = -T + c_1\Omega_2 \tag{14}$$

which possesses an equilibrium point at $\varphi = \varphi_{\text{eq}} = \{(\mu/\mu_0)T_\text{s} + c_1\Omega_2\}/k$. To simplify the analysis, the following nondimensional quantities are introduced:

$$\tau = \omega t, \quad \psi = \varphi - \varphi_{\text{eq}}, \quad \zeta = c_1/(2J_1\omega), \quad \eta = \Omega_2/\omega, \quad \theta = (1 - \mu/\mu_0)T_\text{s}/k, \tag{15}$$

where $\omega = \sqrt{k/J_1}$. Following Jansen [7], the parameters ζ and θ are chosen equal to 0.05 and 4.2, respectively. These values are typical for a drill string that exhibits stick-slip behavior. The nondimensional equation of motion is given by

$$\psi'' + 2\zeta\psi' + \psi = T^*, \tag{16}$$

where a prime denotes a differentiation with respect to τ and $T^* = -\{T + (\mu/\mu_0)T_\text{s}\}/k$.

T^* is given by

$$\begin{cases} -(1 + \mu/\mu_0)T_s/k \le T^* \le \theta & \text{if } \psi' - \eta = 0, \\ T^* = 0 & \text{if } \psi' - \eta < 0, \\ T^* = -2(\mu/\mu_0)T_s/k & \text{if } \psi' - \eta > 0. \end{cases} \tag{17}$$

It is assumed that the drill bit does not rotate backwards and thus $\psi' - \eta = -\varphi_1' \le 0$. T^* can then be approximated by the smooth function

$$\begin{cases} 0 & \text{if } \psi' - \eta \le -4\kappa, \\ -\theta(\psi' - \eta)(\psi' - \eta + 4\kappa)^3/27\kappa^4 & \text{if } \psi' - \eta > -4\kappa, \end{cases} \tag{18}$$

where κ is the accuracy parameter. The arctangent function cannot be used in this case because the dynamic friction coefficient at zero relative velocity is unequal to the static friction coefficient. Figure 6b shows T/k and the smooth approximations with $\kappa = 10^0$, 10^{-1}, and 10^{-2}. Decreasing κ improves the approximation.

In Figure 7a, the stable periodic solutions at $\eta = 4$ are shown for the approximations with $\kappa = 10^0$, 10^{-1}, and 10^{-2}. An 'exact' solution to the discontinuous model is again found by brute force with Hénon's method. The 'exact' solution is shown in Figure 7a by the thick line and is used to investigate the accuracy of the approximations. The relative error e of the approximate solutions is defined by

$$e = \sqrt{\frac{\sum_i(\psi_i - \psi_{\text{exact},i})^2 + \sum_i(\psi_i' - \psi_{\text{exact},i}')^2 + (P - P_{\text{exact}})^2}{\sum_i \psi_{\text{exact},i}^2 + \sum_i \psi_{\text{exact},i}'^2 + P_{\text{exact}}^2}}, \tag{19}$$

where the subscript i denotes $\tau = iP/N$ and $\tau = iP_{\text{exact}}/N$ for the approximate and 'exact' solutions, respectively, P and P_{exact} are the periods of the approximate and 'exact' solutions, respectively, the summations over i are from 0 to $N - 1$, and N is the number of time points. The error is given in Table 4 as a function of κ, where N is chosen equal to 200.

Path following is performed with η as the design variable, starting from the calculated approximate solutions at $\eta = 4$. Figure 7b shows $\max|\psi|$ as a function of η for the approximations with $\kappa = 10^0$, 10^{-1}, and 10^{-2}, and for the 'exact' solution found by brute force (thick line).

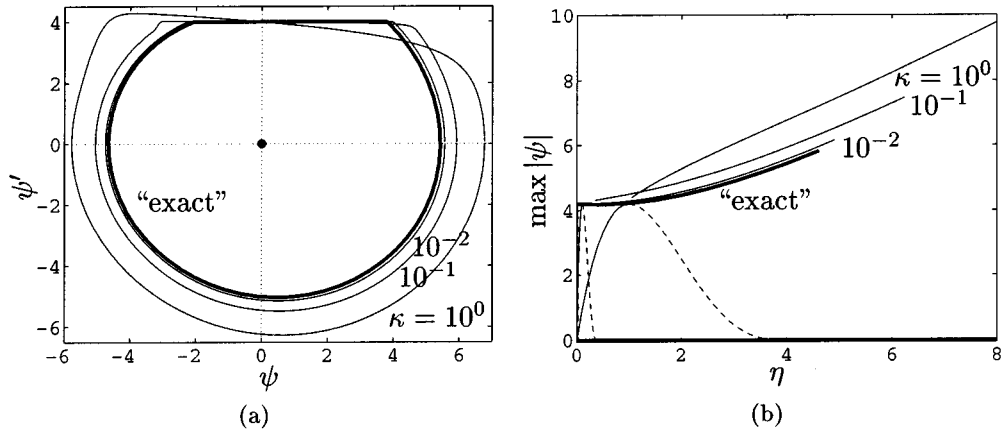

Figure 7. (a) Periodic solution at $\eta = 4$ and (b) max $|\psi|$ as a function of η.

Table 4. Error e of the approximate solutions at $\eta = 4$.

κ	10^0	10^{-1}	10^{-2}	10^{-3}	10^{-4}
e	$3.1 \cdot 10^{-1}$	$9.3 \cdot 10^{-2}$	$2.3 \cdot 10^{-2}$	$5.4 \cdot 10^{-3}$	$1.2 \cdot 10^{-3}$

The equilibrium points of the approximate and discontinuous models, given by

$$\begin{cases} \psi = -\theta\eta(\eta - 4\kappa)^3/27\kappa^4 & \text{if } \eta < 4\kappa, \\ \psi = 0 & \text{if } \eta \geq 4\kappa, \end{cases} \quad \text{and} \quad \psi = 0, \tag{20}$$

respectively, are also shown in Figure 7b, where solid and dashed lines represent stable and unstable branches, respectively. The equilibrium point of the discontinuous model (thick line at $\psi = 0$) is stable for all values of η. For the approximate models, however, there are two values of η (given in Table 5), where the stability of the equilibrium point changes by super and sub-critical Hopf bifurcations. At these super and sub-critical Hopf bifurcations, stable and unstable periodic solutions are born, respectively. The approximate stable periodic solution branches do not reach the super-critical Hopf bifurcation because the step size in the path following algorithm becomes smaller than the user defined minimum. In the positive η-direction, these branches approach a cyclic fold and the step size again becomes too small, so no unstable periodic solution branches are found.

Table 5. Super and sub-critical Hopf bifurcation points.

ε	10^0	10^{-1}	10^{-2}	10^{-3}	10^{-4}
η_{super}	1.02	$1.00 \cdot 10^{-1}$	$1.00 \cdot 10^{-2}$	$1.00 \cdot 10^{-3}$	$1.00 \cdot 10^{-4}$
η_{sub}	3.76	$3.93 \cdot 10^{-1}$	$3.98 \cdot 10^{-2}$	$3.99 \cdot 10^{-3}$	$4.00 \cdot 10^{-4}$

4. Conclusions and Discussion

Using the smoothing procedure to approximate the discontinuous friction forces, systems with dry friction can successfully be modeled in a bifurcation code such as STRDYN. By applying the simple shooting method with a stiff-ODE solver, in combination with the path following algorithm, branches of both stable and unstable periodic solutions can be computed for a changing design variable. The procedure is applied to both 1 and 2-DOF autonomous block-on-belt models and a 1-DOF autonomous drill string model from literature. The calculated stable periodic solutions correspond to the results from the original articles, but in addition unstable solutions branches and an extra stable solution branch are found for the 2-DOF block-on-belt model. The smoothing procedure can also easily be applied to more complex MDOF models, as well as to nonautonomous dynamic systems.

Stick-slip vibrations can also be approximated by the so-called 'alternate friction model' or 'switch model' [8]. This model treats the system as three different sets of ODEs: one for the slip phase, one for the stick phase, and one for the stick-to-slip transition, which can be integrated by any standard ODE-solver. The standard simple shooting method [9], however, cannot be used, because of the discontinuities that arise in the fundamental solution matrix. Leine et al. [8] describe a modified simple shooting method to find periodic solutions with the alternate friction model.

Appendix

A. 'Exact' Solution by Hénon's Method

Equation (2) can be rewritten into the state equation

$$\underset{\sim}{x}' = \underset{\sim}{f}(\underset{\sim}{x}), \tag{21}$$

where a prime denotes a differentiation with respect to τ, $\underset{\sim}{x} = [X \; X']^{\mathrm{T}}$, and, assuming $V_{\mathrm{rel}} \leq 0$, $\underset{\sim}{f}$ is given by

$$\underset{\sim}{f}_1 = \begin{bmatrix} X' \\ -X + 1/(1 - \gamma V_{\mathrm{rel}}) \end{bmatrix} \quad \text{and} \quad \underset{\sim}{f}_2 = \begin{bmatrix} X' \\ 0 \end{bmatrix} \tag{22}$$

in the slip and stick phases, respectively. Equation (21) is integrated by the fourth-order Runge–Kutta scheme

$$\begin{aligned} \underset{\sim}{k}_1 &= \underset{\sim}{f}(\underset{\sim}{x}_i), \\ \underset{\sim}{k}_2 &= \underset{\sim}{f}(\underset{\sim}{x}_i + \frac{1}{2}h\underset{\sim}{k}_1), \\ \underset{\sim}{k}_3 &= \underset{\sim}{f}(\underset{\sim}{x}_i + \frac{1}{2}h\underset{\sim}{k}_2), \\ \underset{\sim}{k}_4 &= \underset{\sim}{f}(\underset{\sim}{x}_i + h\underset{\sim}{k}_3), \\ \underset{\sim}{x}_{i+1} &= \underset{\sim}{x}_i + \frac{1}{6}h(\underset{\sim}{k}_1 + 2\underset{\sim}{k}_2 + 2\underset{\sim}{k}_3 + \underset{\sim}{k}_4), \end{aligned} \tag{23}$$

where h is the time step and $\underset{\sim}{x}_i$ represents $\underset{\sim}{x}$ at $\tau = ih$.

When, during the slip phase, $X'_{i+1} > V_{\mathrm{dr}}$, the last integration step is repeated with the 'inverted' slip equation

$$\frac{\mathrm{d}\underset{\sim}{y}_1}{\mathrm{d}X'} = \underset{\sim}{f}_1^{\mathrm{inv}}(X', \underset{\sim}{y}_1) = \begin{bmatrix} X'/\{-X + 1/(1-\gamma V_{\mathrm{rel}})\} \\ 1/\{-X + 1/(1-\gamma V_{\mathrm{rel}})\} \end{bmatrix}, \tag{24}$$

where $\underset{\sim}{y}_1 = [X\ \tau]^{\mathrm{T}}$ and X' is the independent variable. In one step of the integration scheme

$$\begin{aligned}
\underset{\sim}{k}_1 &= \underset{\sim}{f}_1^{\mathrm{inv}}(X'_i, \underset{\sim}{y}_{1,i}), \\
\underset{\sim}{k}_2 &= \underset{\sim}{f}_1^{\mathrm{inv}}(X'_i + \frac{1}{2}h_1, \underset{\sim}{y}_{1,i} + \frac{1}{2}h_1\underset{\sim}{k}_1), \\
\underset{\sim}{k}_3 &= \underset{\sim}{f}_1^{\mathrm{inv}}(X'_i + \frac{1}{2}h_1, \underset{\sim}{y}_{1,i} + \frac{1}{2}h_1\underset{\sim}{k}_2), \\
\underset{\sim}{k}_4 &= \underset{\sim}{f}_1^{\mathrm{inv}}(X'_i + h_1, \underset{\sim}{y}_{1,i} + h_1\underset{\sim}{k}_3), \\
\underset{\sim}{y}_{1,i+1} &= \underset{\sim}{y}_{1,i} + \frac{1}{6}h_1(\underset{\sim}{k}_1 + 2\underset{\sim}{k}_2 + 2\underset{\sim}{k}_3 + \underset{\sim}{k}_4),
\end{aligned} \tag{25}$$

where $h_1 = V_{\mathrm{dr}} - X'_i$, the slip-to-stick transition is found and the time integration of Equation (23) can be continued.

When, during the stick phase, $X_{i+1} > 1$, the last integration step is repeated with the 'inverted' stick equation

$$\frac{\mathrm{d}\underset{\sim}{y}_2}{\mathrm{d}X} = \underset{\sim}{f}_2^{\mathrm{inv}}(X, \underset{\sim}{y}_2) = \begin{bmatrix} 1/X' \\ 0 \end{bmatrix}, \tag{26}$$

where $\underset{\sim}{y}_2 = [\tau\ X']^{\mathrm{T}}$ and X is the independent variable. In one step of the integration scheme

$$\begin{aligned}
\underset{\sim}{k}_1 &= \underset{\sim}{f}_2^{\mathrm{inv}}(X_i, \underset{\sim}{y}_{2,i}), \\
\underset{\sim}{k}_2 &= \underset{\sim}{f}_2^{\mathrm{inv}}(X_i + \frac{1}{2}h_2, \underset{\sim}{y}_{2,i} + \frac{1}{2}h_2\underset{\sim}{k}_1), \\
\underset{\sim}{k}_3 &= \underset{\sim}{f}_2^{\mathrm{inv}}(X_i + \frac{1}{2}h_2, \underset{\sim}{y}_{2,i} + \frac{1}{2}h_2\underset{\sim}{k}_2), \\
\underset{\sim}{k}_4 &= \underset{\sim}{f}_2^{\mathrm{inv}}(X_i + h_2, \underset{\sim}{y}_{2,i} + h_2\underset{\sim}{k}_3), \\
\underset{\sim}{y}_{2,i+1} &= \underset{\sim}{y}_{2,i} + \frac{1}{6}h_2(\underset{\sim}{k}_1 + 2\underset{\sim}{k}_2 + 2\underset{\sim}{k}_3 + \underset{\sim}{k}_4),
\end{aligned} \tag{27}$$

where $h_2 = 1 - X_i$, the stick-to-slip transition is found and the time integration of Equation (23) can be continued.

References

1. DIANA *User's Manual*, TNO Building and Construction Research, Delft, The Netherlands.
2. Fey, R. H. B., 'Steady-state behaviour of reduced dynamic systems with local nonlinearities', Ph.D. Thesis, Eindhoven University of Technology, Eindhoven, The Netherlands, 1992.
3. Galvanetto, U., Bishop, S. R., and Briseghella, L., 'Mechanical stick-slip vibrations', *International Journal of Bifurcation and Chaos* **5**(3), 1995, 637–651.

4. Hénon, M., 'On the numerical computation of Poincaré maps', *Physica D* **5**, 1982, 412–414.
5. Hindmarsh, A. C., 'ODEPACK, a systematized collection of ODE solvers', in *Scientific Computing*, R. S. Stepleman (ed.), North-Holland, Amsterdam, 1983, pp. 55–64.
6. Ibrahim, R. A., 'Friction-induced vibration, chatter, squeal, and chaos, part II: dynamics and modeling', *Applied Mechanics Reviews* **47**(7), 1994, 227–253.
7. Jansen, J. D., 'Nonlinear dynamics of oilwell drillstrings', Ph.D. Thesis, Delft University Press, Delft, The Netherlands, 1993.
8. Leine, R. I., Van Campen, D. H., and De Kraker, A., 'Stick-slip vibrations by alternate friction models', *Nonlinear Dynamics* **16**(1), 1998, 41–54.
9. Parker, T. S. and Chua, L. O., *Practical Numerical Algorithms for Chaotic Systems*, Springer-Verlag, Berlin, 1989.
10. Popp, K. and Stelter, P., 'Nonlinear oscillations of structures induced by dry friction', in *Nonlinear Dynamics in Engineering Systems*, W. Schiehlen (ed.), Springer-Verlag, Berlin, 1990, pp. 233–240.
11. Van den Steen, L., 'Suppressing stick-slip-induced drillstring oscillations: A hyperstability approach', Ph.D. Thesis, University of Twente, Enschede, The Netherlands, 1997.
12. Van de Vorst, E. L. B., 'Long term dynamics and stabilization of nonlinear mechanical systems', Ph.D. Thesis, Eindhoven University of Technology, Eindhoven, The Netherlands, 1996.